Biosensors and Bioelectronics 49 (2013) 210–215

Contents lists available at SciVerse ScienceDirect

Biosensors and Bioelectronics

journal homepage: www.elsevier.com/locate/bios

Short communication

Facile fabrication of AgNPs/(PVA/PEI) nanofibers: High electrochemical efficiency and durability for biosensors

Han Zhu [b], MingLiang Du [a,b,*], Ming Zhang [a,b], Pan Wang [b], ShiYong Bao [b], LiNa Wang [a], YaQin Fu [a,b], JuMing Yao [a,b]

[a] Key Laboratory of Advanced Textile Materials and Manufacturing Technology, Zhejiang Sci-Tech University, Ministry of Education, Hangzhou 310018, PR China

[b] Department of Materials Engineering, College of Materials and Textile, Zhejiang Sci-Tech University, Hangzhou 310018, PR China

ARTICLE INFO

Article history:
Received 19 February 2013
Received in revised form
2 April 2013
Accepted 15 April 2013
Available online 15 May 2013

Keywords:
Biosensor
Nanofiber
Ag nanoparticles
Electrochemical

ABSTRACT

A novel, facile and green approach for the fabrication of H_2O_2, glutathione (GSH) and glucose detection biosensor using water-stable PVA and PVA/PEI nanofibers decorated with AgNPs by combining an in situ reduction approach and electrospinning technique has been demonstrated. Small, uniform and well-dispersed AgNPs embedded in the PVA nanofibers and immobilized on functionalized PVA/PEI nanofibers indicate the highly sensitive detection of H_2O_2 with a detection limit of 5 μM and exhibit a fast response, broad linear range, low detection limit and excellent stability and reusability.

1. Introduction

The development of materials science has brought great impetus to applied electrochemical fields and many efforts always have been made in finding new materials with good properties to improve electrochemical performances (Feng et al., 2011; Lin and Yan, 2012; Mao et al., 2010; Wang et al., 2012; Trefry et al., 2010). Electrochemical biosensors using various nanomaterials achieve the direct electron transfer between the enzyme and the electrode, which is very important for the fundamental studies and the construction of biosensors (Feng et al., 2011; Wang et al., 2012). However, enzymes often exhibit sluggish electron transfer at conventional electrodes because of unfavorable orientation on the electrode surface or the adsorption of impurities that cause denaturation. (Feng et al., 2011; Myung et al., 2011; Ishikawa et al., 2010; Cella et al., 2010) Therefore, appropriate promoters should be employed to facilitate the electron transfer and retain the bioactivity of immobilized enzymes. With the rapid development of nanotechnology, metal nanoparticles (MNPs) have been extensively used in electroanalysis due to their unique capabilities to enhance mass transport, facilitate catalysis, increase surface area, and control an electrode's microenvironment (Wang et al., 2003; Jin 2012; Sau et al., 2010; Lu et al., 2008; Zhang et al., 2013).

A common challenge in MNPs-based biosensors is controlling the size, dispersion, stability, electrocatalytic activity of the MNPs and finding a convenient synthesis procedure. Recently, nanofibers are intensively applied as substrate materials in the fabrication of advanced intelligent biosensors due to their flexibilities, high specific surface area, high porosity, and good mechanical strength (Wang et al., 2012; Li and Xia 2004; Zhu et al., 2012a, 2012b). Compared with the traditional materials used for biosensors, the combined advantages of biocompatible nanofibers and MNPs would lead to high sensitivity and stability for the biosensing (Yang et al., 2012; Zhong et al., 2012; Huang et al., 2012; Zhu et al., 2012a,b).

Here, we reported a novel strategy for the fabrication of well-dispersed small Ag nanoparticles (AgNPs) embedded in water-stable poly(vinyl alcohol) (PVA) nanofibers and immobilized on the functionalized water-stable PVA/poly(ethyleneimine) (PEI) nanofibers by combining an in situ reduction approach and electrospinning technique, and these novel materials exhibit a highly sensitive detection of H_2O_2, GSH and glucose and possess good stability and repeatability.

2. Material and methods

Details of the materials and methods are given in the Supporting information.

* Corresponding author at: Key Laboratory of Advanced Textile Materials and Manufacturing Technology, Zhejiang Sci-Tech University, Ministry of Education, Hangzhou 310018, PR China. Tel.: +86 571 86843255.
E-mail addresses: psduml@yahoo.com.cn, du@zstu.edu.cn (M. Du).

0956-5663/$ - see front matter © 2013 Elsevier B.V. All rights reserved.
http://dx.doi.org/10.1016/j.bios.2013.04.016

3. Results

A schematic of the fabrication process of AgNPs/PVA and AgNPs/(PVA/PEI) nanofibers is shown in Scheme 1. In the typical experiments for fabricating AgNPs/PVA water-stable nanofibers, PVA solution were firstly mixed with $AgNO_3$ solution, and because of the chelating effect between hydroxyl groups and Ag^+ ions, the abundant hydroxyl groups of the PVA molecular chains could "anchor" Ag^+ ions to form chelate complex. After the addition of the green reductant, epigallocatechin gallate (EGCG), the Ag^+ ions in the chelate complex would grow to AgNPs (Zhu et al., 2012; Zhu et al., 2012). The AgNPs/PVA nanofibers mats were obtained by electrospinning the above precursor and then crosslinked by glutaraldehyde (GA) vapor to gain water stability. As shown in Fig. 1a and b, well-dispersed small AgNPs embedded in PVA nanofibers with a uniformly average diameter of 3.3 ± 0.3 nm have been successfully prepared. Nearly no AgNPs aggregation are observed, indicating the effective protection of PVA molecular chains and EGCG (Zhu et al., 2012a, 2012b).

High-resolution transmission electron microscopy (HRTEM) image of the AgNPs shows the lattice spacing of the (1 1 1) planes of Ag with a spacing of about 0.23 nm (Gu et al., 2009; Metraux and Mirkin 2005; Sun and Xia 2002). The morphology of the water-stable AgNPs/PVA nanofibers is shown in Fig. 1c and d, and compared with the pristine nanofibers before cross-linking (Fig. S1 and S2, average diameter$=410 \pm 60$ nm), uniform and excellent porous fibrous structures are well-retained, except for an obvious increase in the mean fiber diameter (630 ± 73 nm). This can be ascribed to the swelling of the fibers during the GA vapor cross-linking process and the morphology of the as-prepared water-stable nanofibers is better than that the previously reported literatures (Wang et al., 2012; Huang et al., 2012). As shown in Fig. 1(d), small AgNPs can be observed on the surface of PVA nanofibers, and after the immersion in water for 12, 24, 48 and 64 h, the nanofibers still kept excellent porous fibrous structure and no adhesion phenomenon appeared (Fig. S3). In addition, large amount of the small AgNPs still can be observed, indicating the reliability of the water-stable nanofibers (Fig. S3). The UV–vis spectrum of the AgNPs/PVA nanofibers exhibit a strong and sharp surface plasmon resonance (SPR) peak at 419 nm, which is attributed to the isolated spherical AgNPs (Metraux and Mirkin, 2005; Sun and Xia 2002). The sharp SPR peak of AgNPs can also indicate the relative uniformly NPs' size distribution.

It is well known that the smaller the size, the higher the activity of NPs could be. Through the in situ approach in polymer solution and electrospun technique, small and well dispersed AgNPs can be obtained. However, most of the AgNPs are embedded in the PVA nanofibers so that the activity of the AgNPs may be restrained. In order to maximize the opportunity to use the higher activity caused by the small size, another approach for the fabrication of small AgNPs with well dispersion immobilized on the surface of nanofibers has been demonstrated, which is shown in Scheme 1b. In the typical process, the as-prepared PVA/PEI water-stable nanofibers were firstly functionalized with 3-mercaptopropyl-trimethoxysilane (MPTES) to provide sulfhydryl groups, which can chelate with Ag^+ ions and will "anchor" the small AgNPs (Wang et al., 2012; Zhu et al., 2012b). Then the prepared Ag^+/PVA/PEI nanofibers mats were immersed into EGCG solution, after a certain time, the AgNPs/(PVA/PEI) nanofibers were obtained. Fig. 1e and f shows the TEM images of the AgNPs immobilized on the surface of functionalized PVA/PEI nanofibers with a narrow size distribution of about 7.3 ± 0.4 nm. The small AgNPs are uniformly distributed on the surface of nanofibers, except for a few aggregation NPs, which are corresponded with the FE-SEM images in Fig. 1g and h. As shown in Fig. 1g, uniform nanofibers with random orientation and porous fibrous structure were generated with a mean diameter of 508 ± 48 nm (inset in Fig. 1g). The aim of the introduction of PEI is to improve the morphology of the nanofibers and the water stability. At the same condition, after the cross-linking of PVA/PEI nanofibers, the diameter is smaller than cross-linked PVA nanofibers, it is because that the aldehyde groups of GA is able to interact with the amine groups of PEI and the hydroxyl groups of PVA Huang et al. (2012). HRTEM images shown in Fig. 1f were visible with a spacing of about 0.23 nm, which corresponded to the lattice spacing of the (1 1 1) planes of Ag (Gu et al., 2009; Metraux and Mirkin, 2005; Sun and Xia, 2002). Compared with the UV–vis spectrum of AgNPs/PVA nanofibers, the SPR peak has a red-shift and move to 436 nm, indicating the relative bigger size of AgNPs (Metraux and Mirkin, 2005; Sun and Xia 2002).

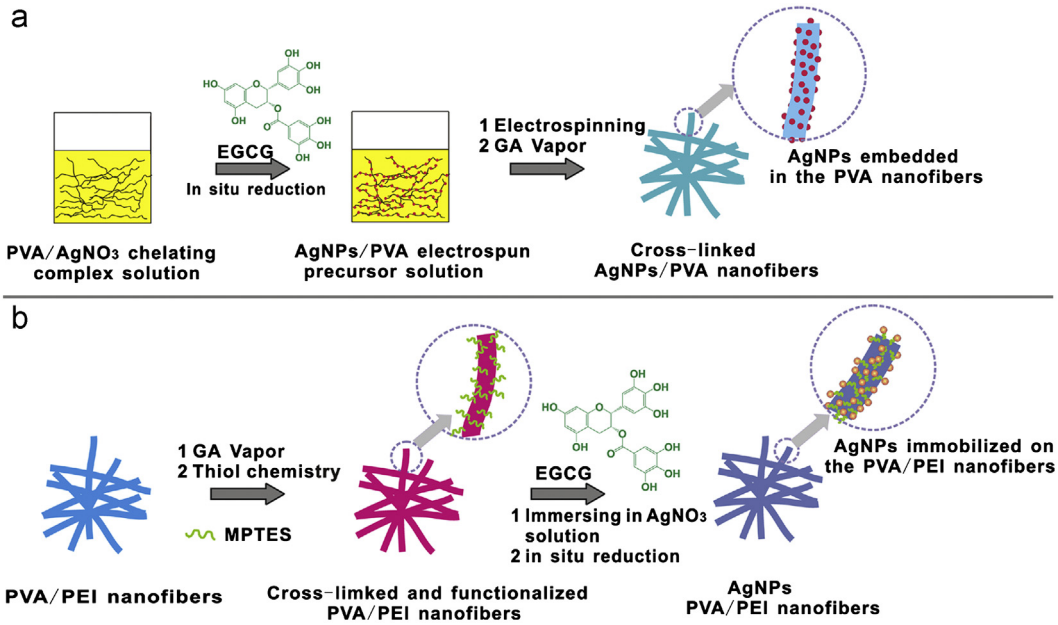

Scheme 1. Schematic of the fabrication process of the (a) AgNPs embedded in the PVA water-stable nanofibers and (b) AgNPs immobilized on the functionalized PVA/PEI water-stable nanofibers.

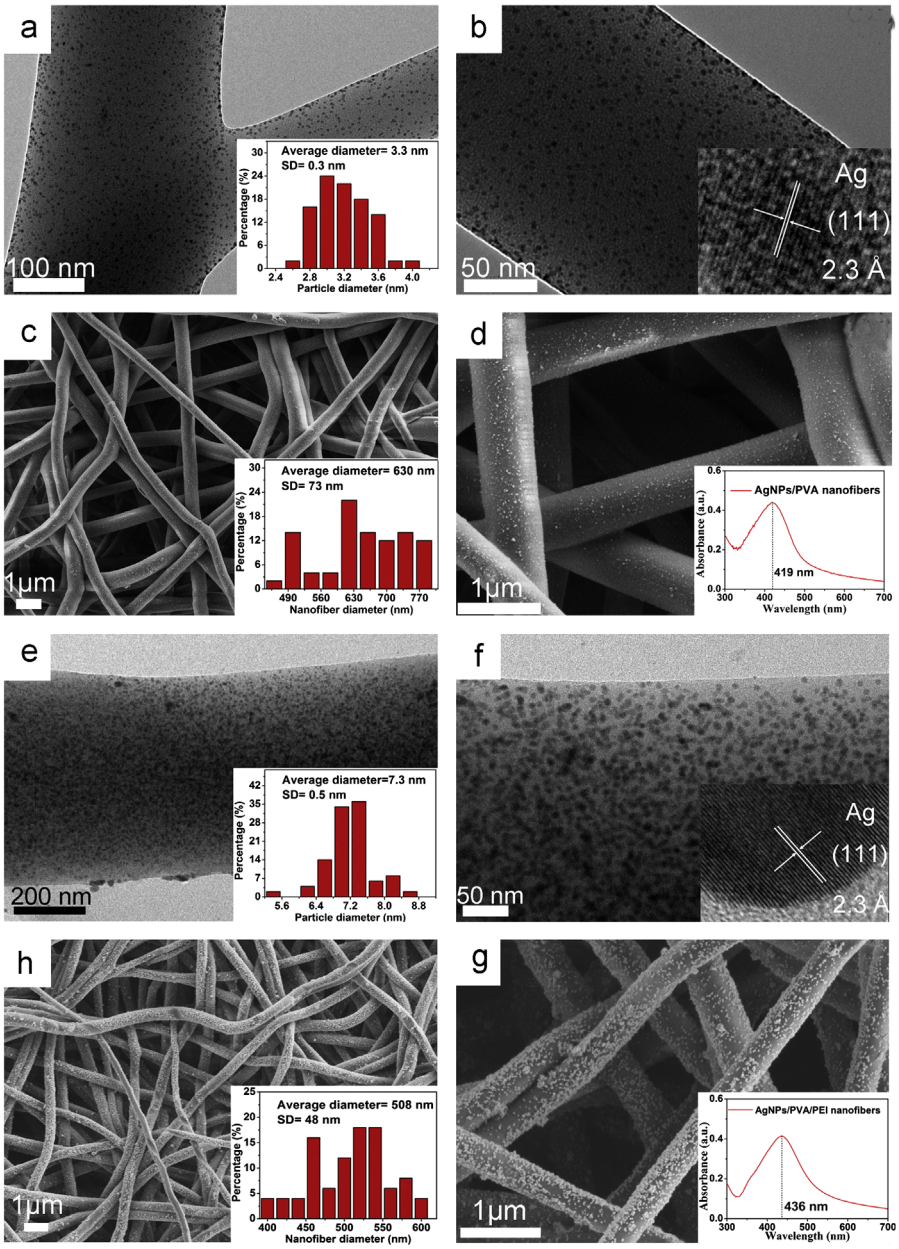

Fig. 1. TEM images of the (a, b) AgNPs/PVA and (e, f) AgNPs/(PVA/PEI) nanofibers. The insets are the corresponding size distribution and HRTEM images of AgNPs. FE-SEM images of (c, d) the AgNPs/PVA and (g, h) AgNPs/(PVA/PEI) nanofibers. The insets are the size distribution of the AgNPs/PVA and AgNPs/(PVA/PEI) nanofibers, and the UV–vis spectra of AgNPs/PVA and AgNPs/(PVA/PEI) nanofibers, respectively.

As shown in Fig. S4F, curve a shows the X-ray diffraction (XRD) spectrum of AgNPs/PVA nanofibers, a broad peak around $2\theta = 19.2^\circ$, corresponding to the (1 0 1) plane of semicrystalline PVA Zhao et al. (2010). The weak diffraction peak located at 37.8° can be indexed as Ag nanocrystal, which correspond to the (1 1 1) planes. It is important to note that compared with curve a, the diffraction peak of Ag (1 1 1) planes become more sharp and the PVA peak become relatively weak. In addition, three new emerging peaks located at 44.4°, 64.7° and 77.3° can also be indexed to the Ag crystal (JCPDS: 04-0783), which correspond to the (2 0 0), (2 2 0) and (3 1 1) planes of face-center cubic silver (Gu et al., 2009; Zhao et al., 2010). The strong peaks of AgNPs indicate the higher ratio of exposed AgNPs than that embedded in PVA nanofibers.

X-ray photoemission spectroscopy (XPS) measurements were performed to reveal the chemical bond formation during the fabrication of AgNPs/PVA and AgNPs/(PVA/PEI) nanofibers. The O 1s chemical states in PVA nanofibers show a strong peak located at 530.3 eV and after the formation of AgNPs, the peak move to 530.0 eV, indicating the chelating effect between the hydroxyls and the AgNPs (Fig. S4A) (Zhu et al., 2012a; Chen et al., 2011). The Ag 3d spectra (Fig. S4B and C) of AgNPs/(PVA/PEI) and AgNPs/PVA nanofibers both demonstrate two significant peaks, located at 371.5, 365.6, 374.0 and 368.0 eV, which are in agreement with the binding energies of Ag $3d_{5/2}$ and Ag $3d_{3/2}$, respectively Zhu et al. (2012b). Compared with the standard binding energy of Ag $3d_{5/2}$ and Ag $3d_{3/2}$, the binding energies of the two kind of nanofibers are lower than bulk Ag (368.2 and 374. 2 eV), indicating the strong interaction among the AgNPs, hydroxyls and sulfydryl groups (Wang et al., 2012; Zhu et al., 2012a). The core level S 2p and Si 2p spectra of AgNPs/(PVA/PEI) nanofibers are shown in Fig. S4D and E. A peak fit is included below the experimental spectrum, presenting two S 2p spin–orbit coupled doublets. The double peak

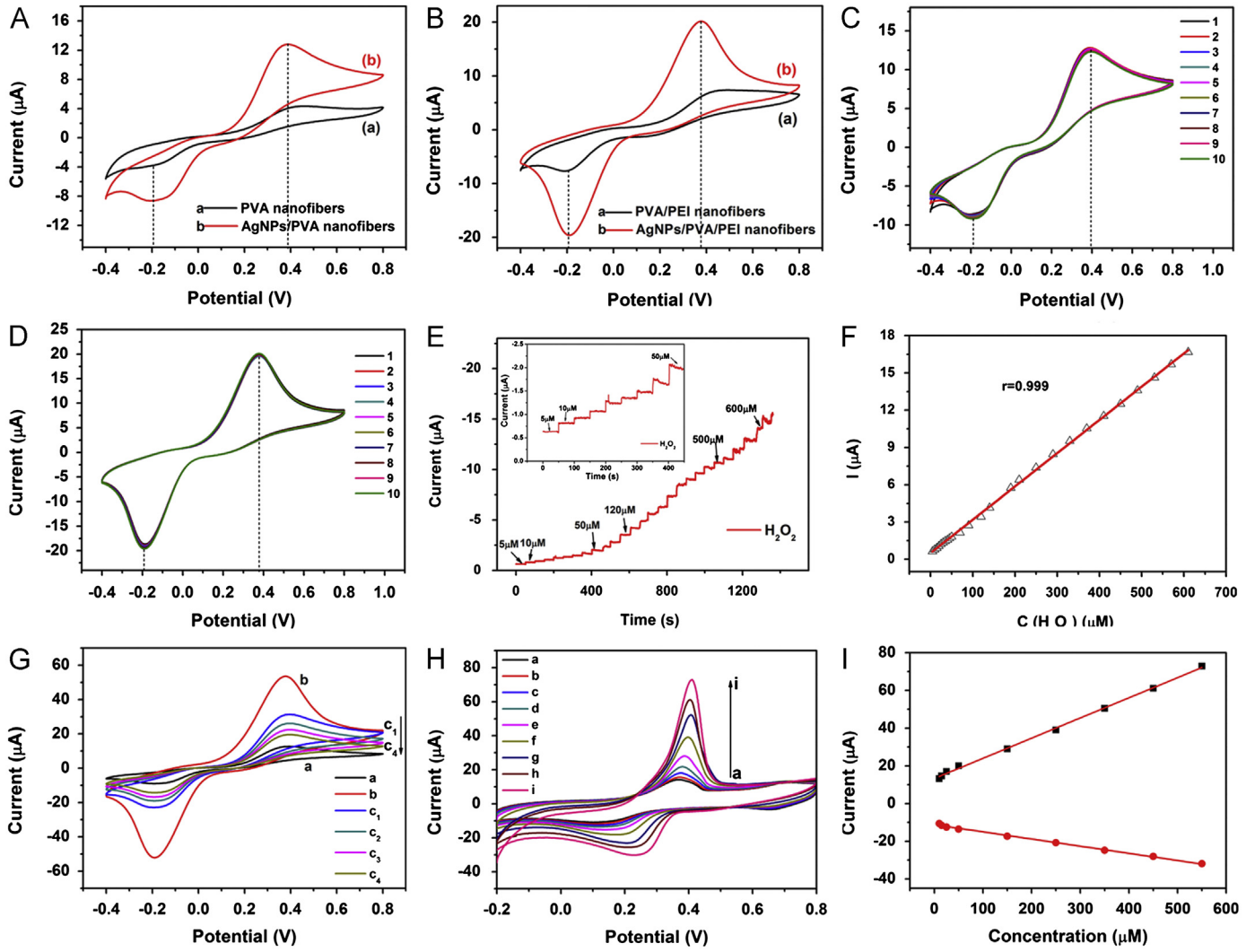

Fig. 2. CVs obtained with (A) AgNPs/PVA and (B) AgNPs/(PVA/PEI) nanofibers functionalized GCE immersed in 1.0 mM HQ in 0.1 M PB (pH 6.8) in the presence of 5.0 mM H_2O_2 (scan rate, 50 mV s^{-1}); The CVs cycles of the prepared (C) AgNPs/PVA/GCE and (D) AgNPs/(PVA/PEI)/GCE at the same conditions; (E) amperometric response of the fabricated HRP/AgNPs/(PVA/PEI)/GCE biosensor to successive addition of different concentrations of H_2O_2 to 1.0 M phosphate buffer (PB) at −0.22 V. Inset shows the response of the biosensor to 5 μM H_2O_2; (F) relationship of calibration curve and linear fitting curve between the current and the H_2O_2 concentration. (G) CVs obtained with AgNPs/(PVA/PEI)/GCE immersed in 1.0 mM HQ in 0.1 M PB (pH 6.8) in the absence of H_2O_2 (a) and in the presence of 10 mM H_2O_2 (scan rate, 50 mV s^{-1}); (c1–c4) same as (b) with 50, 100, 150, 200 μM GSH, respectively; (scan rate, 50 mV s^{-1}). (H) CVs of AgNPs/(PVA/PEI)/GCE electrode in the presence of different concentrations of glucose (5, 10, 15, 25, 50, 150, 250, 350, 450 and 550 μM) at the scan rate of 50 mV s^{-1}. (I) The redox peak currents in CV versus glucose concentration.

is an energy doublet with the $2p_{3/2}$ and $2p_{1/2}$ binding energy peaks positioned at about 162.2 and 163.3 eV, demonstrating the presence of thiolate species (Chen et al., 2011; SelegArd et al., 2010; Khatri et al., 2008).

The formation of thiolate is attributed to interact between sulfur and Ag at the AgNPs. The appearance of characteristic Si 2p peaks at 102.1 eV, Si $2p_{1/2}$ at 97.9 eV, and Si $2p_{3/2}$ at 96.9 eV, which are ascribed to the Si–O, Si–C and Si–Si bondings (Khatri et al., 2008; Wang et al., 2004; Cheung et al., 2003). The presence of Si–O bindings successfully confirmed the grafting between PVA/PEI nanofibers and MPTES. The Schematic picture of the chemical bondings of AgNPs/(PVA/PEI) and AgNPs/PVA nanofibers is shown in Fig. S5.

In this communication, such small, uniform and well-dispersed AgNPs possess high ratio of surface atoms with free valences to the cluster of total atoms and can provide electrochemical reversibility for redox reactions, which is not possible on the bulk metal electrode. The electrochemical behavior of horseradish peroxidase (HRP)/PVA/glassy carbon electrodes (GCE) and HRP/AgNPs/PVA/GCE in the presence of 5.0 mM of H_2O_2 was revealed by the cyclic voltammograms (CVs) (Fig. 2A). Well-defined CVs were obtained in biosensors based on both the HRP/PVA/GCE and HRP/AgNPs/PVA/GCE (Fig. 2A). The redox peak currents of hydroquinone (HQ) (curve a) are about 4.1 and 3.7 μA, with potentials at (0.42 and −0.19 V) and the other redox peak currents (curve b) are about 8.5 and 12.5 μA, with potentials at (0.38 and −0.20 V), respectively. An obvious increase of the peak-to-peak separation was observed, indicating that the AgNPs can successfully promote the HRP embedded in the AgNPs/PVA nanofibers. In the same condition, compared with the redox peak currents in PVA/PEI nanofibers electrode (7.2 and −7.4 μA), the AgNPs/(PVA/PEI) nanofibers electrode obtain a significant increase (20.3 and −20.1 μA), which is ascribed to the relative higher content of exposed AgNPs. It should be noted that even the AgNPs embedded in PVA nanofibers possess the smaller size and higher specific surface area, but the AgNPs on PVA/PEI nanofibers have higher ratio of exposed AgNPs, which also can be demonstrated by XRD characterization (Fig. S4A).

Therefore, much more AgNPs could take part in the reactions, leading to the relative higher electrocatalytic activity. The reusability and recyclability are crucial issues for practical applications, especially for the costly rare and noble metals. The fabricated AgNPs/PVA and AgNPs/(PVA/PEI) nanofibers electrodes used for 10 times were compared by the CV curves (Fig. 2C and D). The reproducibility of the same electrode in the measurements,

expressed as the relative standard deviation (RSD), was less than 3.3% for 10 successive experiments in the presence of 5.0 mM of H_2O_2. The redox peaks are almost the same, indicating the excellent stability and reusability of fabricated AgNPs/PVA and AgNPs/(PVA/PEI) nanofibers electrodes. Considering the good reduction current (20.1 μA) caused by HQ in the presence of H_2O_2, we choose the AgNPs/(PVA/PEI) nanofibers mats as the electrode to accurately determine the concentration of H_2O_2. Fig. 2E shows the amperometry response and calibration curve of steady state current vs. concentration of H_2O_2. Stepped increases of the amperometric reduction currents were observed with the addition of H_2O_2 at a constant potential of −0.22 V. The current response of the sensors was rapidly enhanced and approached about 98% of its steady state current within 1 s, which is much shorter than that in the previous reports (Chen et al., 2008; Zhu et al., 2006; Lei et al., 2004). The rapid electrode response to the change of the H_2O_2 concentration is attributed to the fast diffusion of the H_2O_2 into the AgNPs/PVA/PEI nanofibers network structures and the surface of small AgNPs. Fig. 2F shows a linear relationship with the concentration of H_2O_2 (5–0.6 mM) with the correlation coefficient of 0.999. The detection limit of 0.6 mM was estimated at a signal-to-noise ratio of 3. The results indicated the HRP/AgNPs/(PVA/PEI)/GCE has much higher catalytic ability for the reduction of H_2O_2 than that in the previous reports (Chen et al., 2008; Zhu et al., 2006; Lei et al., 2004), and the high sensitivity may result in the excellent biocompatible microenvironment of the AgNPs/(PVA/PEI) nanofibers around the enzyme.

Beside H_2O_2, glutathione (GSH) and glucose are widely found in all forms of life and play essential roles in the health of organisms, and therefore, they were also used as model compounds in our experiments to testify the electrochemical activity and flexibility of the biosensor. Fig. 2G shows the CVs of GSH using HRP/AgNPs/(PVA/PEI)/GCE as electrode and in the presence of 1 mM HQ, there appears a pair of redox peaks (curve a). After the addition of 5 mM H_2O_2, the amperometric reduction currents increase (curve b) and upon addition of 50 μM GSH, the reduction current decreases dramatically (curve c1). With the further increase of the concentration of GSH (curve c1 to curve c2) the decrease is enhanced. It is well-known that with the assists of H_2O_2, the HRP can easily convert HQ to benzoquinone (BQ), and then the benzoquinone is subsequently reduced back to HQ by a rapid reaction involving the acceptance of two electrons from the electrode (Taraban et al., 1997; Liu et al., 2009). The model compound, GSH, is an inhibitor (reduced thiols, R-SH), and it may react with BQ to produce a reduced adduct (quinoid–thiol) (Huang et al., 2002; Elyacoubi et al., 2006) and lead to less BQ derivatives reaching the electrode surface, which can decrease the reduced peak current of HQ. Because of the reduced thiols suppression of the mediator recycling process and inhibition of the activity of HRP, a reduced thiol biosensor can be obtained. Fig. 2H and I shows the electrochemical responses of different concentrations of glucose using HRP/AgNPs/(PVA/PEI)/GCE as an electrode. It can be observed that the redox peaks increase linearly with increasing glucose concentration from 5 μM to 550 μM. The AgNPs/(PVA/PEI) nanofibers modified electrodes exhibit superior performance in the detection of H_2O_2 as compared to the previously reported literatures (Chen et al., 2008; Zhu et al., 2006; Lei et al., 2004; Luo et al., 2009). After storage at 4 °C in a refrigerator for 3 months, the response of H_2O_2 and glucose decrease slightly compared with the fresh biosensor, indicating good durability and stability of the biosensor (Fig. S6).

4. Conclusions

In summary, we have demonstrated a novel, facile and green approach for the fabrication of H_2O_2 detection biosensor using water-stable PVA and PVA/PEI nanofibers decorated with AgNPs by combining an in situ reduction approach and electrospinning technique. Two methods were used to synthesize small, uniform and well-dispersed AgNPs embedded in the PVA nanofibers and immobilized on functionalized PVA/PEI nanofibers. The fabricated HRP/AgNPs/(PVA/PEI) biosensor allowed the highly sensitive detection of H_2O_2, GSH and glucose and exhibited a fast response, broad linear range, low detection limit and excellent stability and reusability. The response and redox peak currents increase with the increase of the ratio of exposed AuNPs. The feasible process and high detection sensitivity of the biosensor based on AgNPs decorated PVA/PEI nanofibers may pave the way in developing a new film support-enzyme hybrid substrate material for biosensors or bioelectrocatalysts.

Acknowledgment

We acknowledge the support of the project of the National Natural Science Foundation of China (NSFC) (51243001) and the 521 Project of Zhejiang Sci-Tech University.

Appendix A. Supporting information

Supplementary data associated with this article can be found in the online version at http://dx.doi.org/10.1016/j.bios.2013.04.016.

References

Cella, L.N., Chen, W., Myung, N.V., Mulchandani, A., 2010. Journal of the American Chemical Society 132, 5024–5026.
Chen, A., Kafi, A.K.M., Wu, G., 2008. Biosensors and Bioelectronics 24, 566–571.
Chen, J.J., Struk, K.N., Brennan, A.B., 2011. Langmuir 27, 13754–13761.
Cheung, M.K.L., Trau, D., Yeung, K.L., Carles, M., Sucher, N.J., 2003. Langmuir 19, 5846–5850.
Elyacoubi, A., Zayed, S.I.M., Blankert, B., Kauffmann, J.M., 2006. Electroanalysis 18, 345–350.
Feng, X.M., Li, R.M., Ma, Y.W., Chen, R.F., Shi, N.E., Fan, Q.L., Huang, W., 2011. Advanced Functional Materials 21, 2989–2996.
Gu, C.D., Cheng, C., Huang, H.Y., Wong, T.L., Wang, N., Zhang, T.Y., 2009. Crystal Growth and Design 9, 3278–3285.
Huang, T.H., Kuwana, T., Warsinke, A., 2002. Biosensors and Bioelectronics 17, 1107–1113.
Huang, Y.P., Ma, H., Wang, S.G., Shen, M.W., Guo, R., Cao, X.Y., Zhu, M.F., Shi, X.Y., 2012. ACS Applied Materials and Interfaces 4, 3054–3061.
Ishikawa, F.N., Curreli, M., Olson, C.A., Liao, H.I., Sun, R., Roberts, R.W., Cote, R.J., Thompson, M.E., Zhou, C.W., 2010. ACS Nano 4, 6914–6922.
Jin, Y.D., 2012. Advanced Materials 24, 5153–5165.
Khatri, O.P., Adachi, K., Murase, K., Okazaki, K., Torimoto, T., Tanaka, N., Kuwabata, S., Sugimura, H., 2008. Langmuir 24, 7785–7792.
Lei, C.X., Hu, S.Q., Gao, N., Shen, G.L., Yu, R.Q., 2004. Bioelectrochemistry 65, 33–39.
Li, D., Xia, Y.N., 2004. Advanced Materials 16, 1151–1170.
Lin, P., Yan, F., 2012. Advanced Materials 24, 34–51.
Liu, L.J., Xi, F.N., Zhang, Y.M., Chen, Z.C., Lin, X.F., 2009. Sensors and Actuators B: Chemical 135, 642–649.
Lu, J., Do, I., Drzal, L.T., Worden, R.M., Lee, I., 2008. ACS Nano 2, 1825–1832.
Luo, S.L., Zeng, X.D., Li, X.F., Liu, X.Y., Liu, Y., Kong, B., Yang, S.L., Wei, W.Z., 2009. Biosensors and Bioelectronics 25, 896–900.
Mao, S., Lu, G.H., Yu, K.H., Bo, Z., Chen, J.H., 2010. Advanced Materials 22, 3521–3526.
Metraux, G.S., Mirkin, C.A., 2005. Advanced Materials 17, 412–415.
Myung, S., Solanki, A., Kim, C., Park, J., Kim, K.S., Lee, K.B., 2011. Advanced Materials 23, 2221–2225.
Sau, T.K., Rogach, A.L., Jackel, F., Klar, T.A., Feldmann, J., 2010. Advanced Materials 22, 1805–1825.
SelegArd, L., Khranovskyy, V., Soderlind, F., Vahlberg, C., Ahren, M., Kall, P.O., Yakimova, R., Uvdal, K., 2010. ACS Applied Materials and Interfaces 2, 2128–2135.
Sun, Y.G., Xia, Y.N., 2002. Science 298, 2176–2179.
Taraban, M.B., Leshina, T.V., Anderson, M.A., Grissom, C.B., 1997. Journal of the American Chemical Society 119, 5768–5769.
Trefry, J.C., Monahan, J.L., Weaver, K.M., Meyerhoefer, A.J., Markopolous, M.M., Arnold, Z.S., Wooley, D.P., Pavel, I.E., 2010. Journal of the American Chemical Society 132, 10970–10972.
Wang, J., Musameh, M., Lin, Y.H., 2003. Journal of the American Chemical Society 125, 2408–2409.

Wang, J., Yao, H.B., He, D., Zhang, C.L., Yu, S.H., 2012. ACS Applied Materials and Interfaces 4, 1963–1971.

Wang, Y., Tang, Z.Y., Liang, X.R., Liz-Marzan, L.M., Kotov, N.A., 2004. Nano Letters 4, 225–231.

Yang, S.Y., Liu, Y.M., Tan, H., Wu, C., Wu, Z.Y., Shen, G.L., Yu, R.Q., 2012. Chemical Communications 48, 2861–2863.

Zhang, Z.H., Zhang, L.B., Hedhili, M.N., Zhang, H.N., Wang, P., 2013. Nano Letters 13, 14–20.

Zhao, L.N., Yang, D.Y., Dong, M.D., Xu, T., Jin, Y., Xu, S.L., Zhang, F.Z., Evans, D.G., Jiang, X.Y., 2010. Industrial and Engineering Chemistry Research 49, 5610–5615.

Zhong, X., Yuan, R., Chai, Y.Q., 2012. Chemical Communications 48, 597–599.

Zhu, H., Du, M.L., Zou, M.L., Xu, C.S., Li, N., Fu, Y.Q., 2012a. Journal of Materials Chemistry 22, 9301–9307.

Zhu, H., Du, M.L., Zou, M.L., Xu, C.S., Fu, Y.Q., 2012b. Dalton Transactions 41, 10465–10471.

Zhu, J.H., Cai, W.Y., Xu, Q., Zhao, X.N., Chen, H.Y., 2006. Chemistry of Materials 18, 279–284.